EURASIAN PHYSICAL TECHNICAL JOURNAL

2024, Volume 21, No.4 (50)

https://doi.org/10.31489/2024No4/79-87

Received: 17/06/2024 Revised: 19/10/2024 Accepted: 18/12/2024 Published online: 25/12/2024

Original Research Article

Open Access under the CC BY -NC-ND 4.0 license

UDC 53.083.7:621.396

DESIGN OF SOFTWARE DEFINED RADIO OF GROUND STATION FOR RECEIVING NANO-SATELLITES IMAGE DATA IN S-BAND

Baktybekov K.S.*, Bochkova E.N., Korol V.V., Murushkin M.S., Zhumazhanov B.R.

Ghalam LLP, Astana, Kazakhstan

*Corresponding author: k.baktybekov@ghalam.kz

Abstract. *This paper presents results for design, production and implementation of a ground station for transmitting and receiving information in the S-band for low-orbital nanosatellites for remote sensing of the Earth. A distinctive feature of the solution is that it uses universal low-cost Software Defined Radio hardware platforms based on programmable logic arrays and transceivers, such as the AD9361. Computational resources are saved by usage of a FIR filter with real coefficients and a carrier signal with a symmetrical impulse response, as well as a frequency converter using the CORDIC algorithm, which provides an efficient solution in terms of field programmable gate arrays resources. This work computes total and useful data transfer rates, as well as the required ratio of the energy of one message bit to the value of the power spectral density of the equivalent noise when used for encoding and modulation of a standard DVB-S2 MODCOD signal. Evaluation of the parameters of the Software Defined Radio field programmable gate arrays transceiver showed that it can be used in both the S and X frequency bands without significant changes in hardware, which can significantly reduce the cost of the ground station.*

Keywords: ground station, software defined radio, nanosatellite, satellite antenna, field programmable gate arrays, coding, modulation, line communication.

1. Introduction

Conventional radio systems predominantly utilize hardware-centric approaches, which offer limited adaptability in software. These solutions are distinguished by the elevated cost, intricating development process, and labor-intensive adjustment, lacking the capability for flexible system reconfiguration. Software Defined Radio (SDR) offers a programmable implementation of numerous functions compared to traditional architecture-based systems. SDR technology can be utilized for both transceivers on satellites and ground stations. The application of SDR for ground stations, in particular, in the field of remote sensing, was demonstrated in the paper [1], where X-band radio station tracking NOAA-20, Suomi-NPP, Terra, Aqua, and other low-orbit satellites was considered. The ground station architecture used by the European Space Agency was upgraded through the integration of software-defined radio technology. Based on this system, the sampling functions were implemented, reaching a rate of 8 Gsym/s, and digital conversion of the radio signal was realized in S- and X-bands [2].

Extensive investigation into the functionalities of SDR for satellite communications was initiated by the National Aeronautics and Space Administration (NASA) [3]. The research was focused on the realization of following operations onboard the spacecraft that are traditionally executed at ground stations. For example, scheduling of communication sessions and calculation of spacecraft antenna angles were discussed. Moreover, the possibility of obtaining adaptative data rate, modulation, and error-correcting coding in

response to fluctuations in communication conditions was explored [4]. The flexibility of SDR-based solutions allows systems to be reconfigured accounting for different effects such as variations in noise temperature, phase offset, and Doppler shift [5].

SDR technologies can offer advantages for low-orbit spacecraft due to due to their ability to compensate for the Doppler effect, which has a significant impact on low-orbit missions [6]. In such scenarios, SDR and specialized software such as GNURadio offer opportunities that surpass the traditional radio hardware architecture, facilitating simplified Doppler compensation for telemetry taking into account the position of the ground station [7]. SDR finds its most common applications among small satellites and ground stations which are often referred to as university projects [8-14]. The peculiarity of solutions for small satellites lies in the utilization of universal inexpensive SDR hardware platforms based on Field Programmable Gate Arrays (FPGA) and chip-based transceivers, such as AD9361.

Software-defined radio finds application in high data rate communication particularly for meteorological satellite systems, which are characterized by high-speed transmission of satellite images. This objective can be achieved even utilizing on universal SDR hardware platforms and open-source code [15-17].

2. Design SDR technology

SDR has the potential to revolutionize approaches in the field of scientific research on satellite communications and Earth sensing. One of the important functionalities provided by SDR is the ability to remove data anomalies from the payload or communication system. Additionally, this technology reduces development costs by designing adaptive, versatile space platforms that enable meeting specific mission requirements. Owing to the use of FPGA, signal processing across multiple frequency bands, filtering procedure, adaptive modulation, and encoding schemes can be executed without significant hardware alterations. Moreover, it becomes possible to transmit and receive signals across various radio protocols and update software of on-board systems during their mission in orbit.

The radio system based on SDR for the ground station was developed. The hardware platform is manufactured by Luowave. This system provides various functions, including modulation, demodulation, and decoding of digital signals. The following modulation schemes are selected for communication links: QPSK for service telemetry, CPFSK for telecommands, and 8PSK for payload data. Communication can be conducted in S and X bands, supporting different polarizations.

Figure 1 depicts a block diagram of the developed software, which is responsible for signal processing. A debugging setup intended for the development process of digital signal processing algorithms consists of the Ettus N321 SDR and the Xilinx Zynq UltraScale+ MPSoC XCZU9EG FPGA debugging board from Alinx. The integrated development environment is "Vivado" from Xilinx, with Verilog as the hardware description language. The operation system is built for the ARM Cortex-A53 processor using the PetaLinux distributive. This tool facilitates step-by-step debugging of the FPGA and allows real-time monitoring of the correct operation of the circuits and automatic testing of each individual functional block.

Testbench consisted of software part based on GNU radio and the debug board as hardware part. The testing scheme represents two signal paths from a common source. In the first case the signal is processed by GNU radio tool and is demonstrated as a reference on a spectrum analyzer. In the second case the signal goes through FPGA on the debag board and is received by second port of the spectrum analyzer.

Next, one of the important components of a satellite communication system is a Doppler compensation block, which is especially critical for the LEO satellites, is described. The motion of a spacecraft relative to a ground station leads to the signal carrier frequency shift in the frequency spectrum due to the Doppler effect. For example, for a signal operating at frequency of 8.2 GHz, the frequency variation lies in the range of 191 kHz to -191 kHz during the time the spacecraft in sight of the ground station passing from horizon to zenith.

The traditional method of Doppler frequency shift compensation consists of mixing the incoming signal with the signal from the local oscillator (LO). The frequency of the LO is dependent on the range rate and satellite trajectory and is calculated from the spacecraft flight program. After the mixer the resulting frequency is corrected compensating Doppler effect.

The Doppler-corrector mixer with a controlled master oscillator was implemented according to the CORDIC algorithm, which allows to reduce the calculation of complex functions to a cycle of addition and shift operations [18]. The Doppler corrector block receives this value via the PS-PL interface and shifts the spectrum of the received signal. Absence of direct synchronization of a transmitter and a receiver leads to a frequency error. Moreover, there is an inaccuracy in prediction of Doppler compensation frequency and

additional frequency offset due to atmosphere effect. To compensate this frequency errors and enhance the modulation quality the frequency correction unit based on band edge filters is applied [19].

The operation principle of the edge filter circuit is to maintain the symmetry of the carrier spectrum relative to zero. To estimate the carrier frequency offset, the passbands of the edge bandpass filters correspond to the lower and upper limits of the carrier frequency spectrum. There is a divergence in power indicators at the output of bandpass filters for the lower and upper boundaries of the spectrum when the spectrum shifts. When the carrier frequency deviates, a signal is sent from the master oscillator to the mixer to compensate for the frequency error.

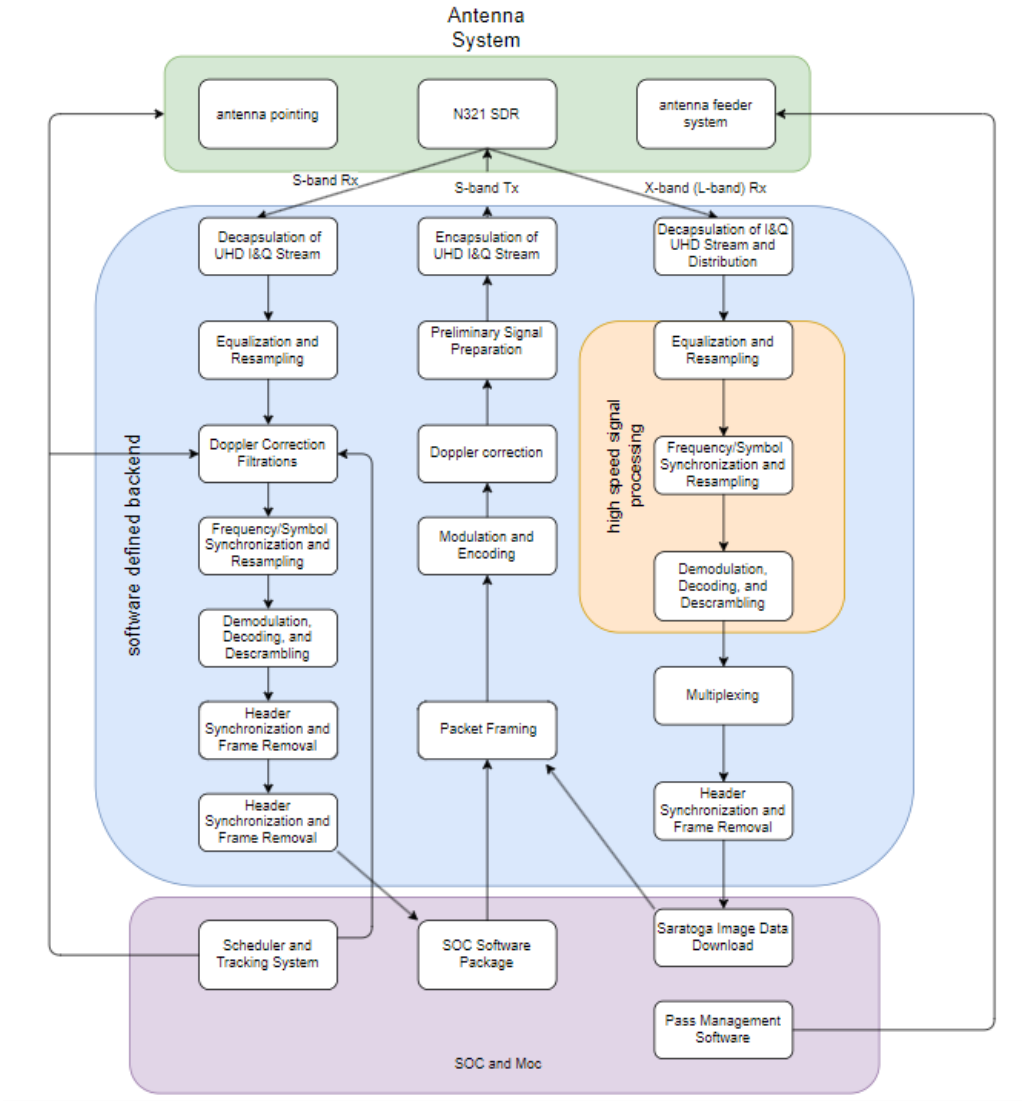

Fig.1. Block diagram of software for SDR platform.

The frequency correction block on the FPGA, as for the Doppler corrector is implemented, using the CORDIC algorithm. The correction block includes a mixer, a controlled master oscillator and edge filters based on FIR filters. Edge filters for the upper and lower boundaries of the spectrum have the same shape of the amplitude-frequency response, which is shifted in the positive and negative directions. Thus, the filters have complex coefficients. Implementing complex coefficient FIR filters on an FPGA means doubling the number of filters, with half having real coefficients and the other half having imaginary coefficients. The filtering procedure involves a multiplication operation for each filter coefficient, which when doubling the number of filters leads to the use of large FPGA resources. To save computational resources, we used a FIR filter with real coefficients and a carrier signal with a symmetrical impulse response and a frequency converter using the CORDIC algorithm. This provided a more efficient solution in terms of FPGA resources.

The above algorithm made it possible to implement Doppler correction of the received signal in order to

fix the carrier frequency. This allows you to move on to the next stage of signal reception - symbol synchronization. Symbol synchronization is the process of adjusting the timing of readings on the receiver with the transmitter timing. The source of timing pulses at the reception is the ADC timing generator, which does not have a direct connection with the transmitter timing generator. Therefore, timing data is extracted directly from the received signal (Figure 2).

The impulse responses of Nyquist filters as symbols were used, namely a filter with a raised cosine response. Nyquist filters are a trade-off between signal bandwidth and intersymbol interference. Those. with a fairly compact form of the signal spectrum, its pulses do not interfere with each other at zero points when they are located on a time interval that is a multiple of the symbol period. The zero values of the pulses are periodic and follow every interval of the symbol period. Outside these null points, pulses overlap each other and interfere with accurate recognition, intersymbol interference increases. The task of symbol synchronization comes down to finding these zero points of the pulse sequence and extracting information about the meaning of the symbol from them.

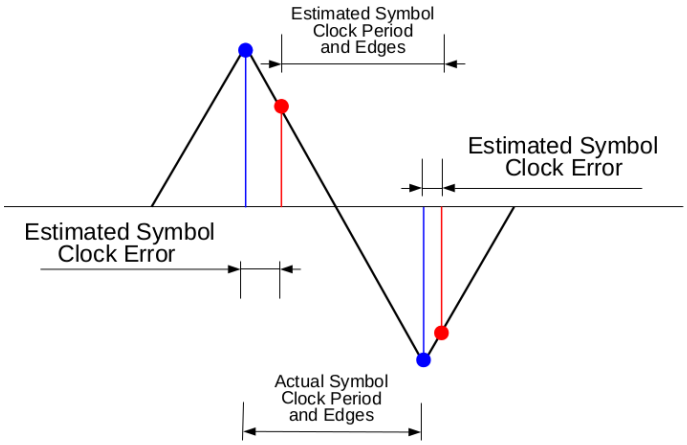

Fig.2. Symbol synchronization scheme.

It should be noted that the receiver operates according to an optimal scheme with a matched filter. This means that a correlation circuit based on a matched filter is used on the receiving side, i.e. the receiver filters out a signal of a certain shape, increasing the reliability of the decision made. The matching of the transmitter and receiver in the signal shape is achieved by using filters with the characteristic of the root of the square raised cosine RRC. Two RRC filters connected in series form a filter with the raised cosine characteristic mentioned earlier. Thus, the RRC filter solves two important problems: it provides optimal reception using a matched filter and minimizes intersymbol interference with a compact signal spectrum.

Digitization at the receiver with a sampling rate higher than the symbol frequency by SPS times is called the number of samples per symbol. Increasing this parameter allows you to find among the readings the one that is as close as possible to the zero point of the pulse. The larger the SPS, the higher the resolution of the time sequence, the higher the accuracy. However, SPS improvement is limited by the performance of the A/D converter and downstream circuitry. Therefore, increasing the resolution of the time sequence of a signal can be achieved by interpolation.

One of the interpolation options is the use of a set of matched filters, the impulse responses of which are identical, only differing in the shift in time space [20]. The filters have the same amplitude-frequency response, but the phase-frequency response differs by a certain amount of group delay time, which is less than the sampling period of the number of filters in the group. Thus, increasing the resolution of the time sequence is achieved by dividing the sampling period into the number of parallel working filters, and the choice of the reference position is achieved by selecting the appropriate filter from the group. Filters are grouped by increasing group delay time, so the time offset becomes equivalent to the filter index. This circuit has a finite number of filters, so the limited resolution of such an interpolator leads to a fixed error.

The ZCTED (Zero-Crossing Timing Error Detector) algorithm is used to estimate the inaccuracy of reference time with symbol time. This method determines the zero-crossing point on the eye diagram and, by analyzing the input sequence, produces a synchronization error signal. This signal is used in a feedback loop to influence the interpolator. In this way, the filter from the group and the sample from the SPS are selected

that corresponds to the minimum ZCTED error. A symbolic synchronization scheme using a group of FIR filters and a ZCTED error analyzer allowed us to develop an FPGA design that has sufficient performance and is acceptable in terms of resource costs.

3. Link budget calculation for S-band uplink and downlink

The link budget is calculated for the described ground station communicating with a LEO satellite. The basic idea of determining the radio link budget derives from the Friis equation, which relates characteristics of a transmitter and receiver and signal propagation path between them. The link budget analysis theoretically estimates the performance of the communication link by accounting for the most critical power gains and losses of the signal. In digital communication, the analysis results in the evaluation of such link quality characteristics as Eb/N0 - the ratio of received energy per bit to spectral noise density. The amount of energy per bit exceeding the noise level is directly proportional to the probability of an error in the bit value determination. For this reason, in communication theory, the E_b/N_0 ratio is defined for a certain bit error rate (BER). The considered radio link operates in the S-band frequency range and involves transmitting telemetry and payload data and receiving telecommands. Two different signal configurations are considered: the first one refers to digital modulation and the second one corresponds to the digital satellite transmission standard, DVB-S2. For the second case full and useful data rates are estimated. The calculations are performed for the defined signal modulations as mentioned above: QPSK for telemetry, 8PSK for payload data, and CPFSK for telecommands. The transmitter symbol rate ranges from 1 *kbit/s* to 500 *kbit/s*.

The downlink includes telemetry transmission and high-rate channel for the payload data transmission. The telemetry signals are modulated by using QPSK scheme where one symbol corresponds to 2 bits, with the required level E_b/N_0 equaling to 10.6 *dB* at BER=10^{-6}. At the same time, using 8PSK modulation 1 symbol of the message corresponds to 3 bits of information, with E_b/N_o level being equal to 14 *dB* at BER=10^{-6}. Table 1 below presents bit rate and required E_b/N_o ratios for QPSK and 8PSK modulations if the symbol rate is leveled to 100 *ksym/s*.

Table 1. Full data rate, useful data rate and E_b/N_0 for QPSK и 8PSK modulations.

Modulation	Symbol rate, [*ksym/s*]	Data rate, [*kbit/s*]	E_b/N_0 at BER=10^{-6} , [*dB*]
QPSK	100	200	10.6
8PSK	100	300	14

Enhanced coding and modulation schemes are implemented in the DVB-S2 standard, to reduce the required Eb/No level and achieve higher bit rates without increasing the signal power [21]. Table 2 demonstrates the total bit rate, useful bit rate, and required E_b/No ratio for several modulation and coding configurations according to DVB-S2. As shown, using the standard allows for achieving a high bit rate at a moderate level of required energy per bit. For example, a bit rate of 1.5 *Mbit/s* can be obtained using 8PSK modulation with a 2/3 coding rate at an Eb/No level of 3.65 *dB*.

Table 2. Full and useful data rate and required Eb/No for different MODCOD according to DVB-S2

MODCOD	Symbol rate, [*ksym/bit*]	Full bit rate, [*kbit/s*]	Useful bit rate, *[kbit/s*]	E_b/No, [*dB*]
QPSK 3/4	100	200	148.7	2.31
QPSK 2/3	100	200	132.2	1.89
QPSK 3/4	500	1000	740	2.31
QPSK 2/3	500	1000	660	1.89
8PSK 2/3	100	300	200	3.65
8PSK 2/3	500	1.5000	1000	3.65

The downlink budget is calculated using the following parameters after determining the required power level for reliable communication, the transmitter output power is 1W, the ratio of gain to the effective noise temperature of the ground station (G/T) is 12 *dB/K*, and the operating frequency is 2.3 *GHz*. The orbit altitude is 600 *km*, and the ground station is located in Astana. A single circularly polarized patch antenna with a maximum gain of 4 *dB* is utilized as the transmitting satellite antenna. Signal attenuation due to

pointing inaccuracy and polarization distortion is assumed to be 0.5 *dB* each, respectively. Additionally, a loss of 3 *dB* in the transmitter and antenna feeder path is taken into account. Atmospheric attenuation for the selected ground station is considered according to the recommendations of the International Telecommunication Union (ITU). The equivalent isotopically radiated power (EIRP) is defined as the product of the gain of the transmitting antenna in a given direction and the output radiated power. EIRP can be calculated using the Friis transmission equation. The calculated EIRP value for an output power of 1*W* and the considered patch antenna is shown in Figure 3.

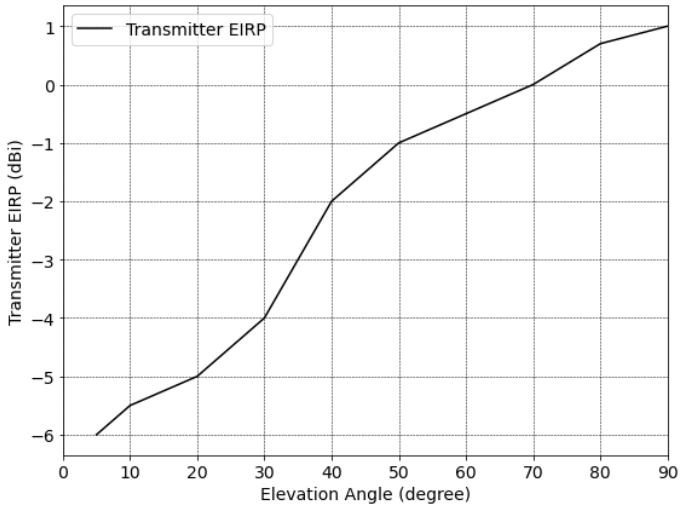

Fig.3. EIRP of the satellite antenna for downlink.

Attenuation due to free space signal propagation from the satellite to the ground station is calculated as a function of the elevation angle. The results are presented in Figure 4. The next step involves obtaining the E_b/N_o level, taking into account the calculated EIRP, free space attenuation, atmospheric loss, and other losses.

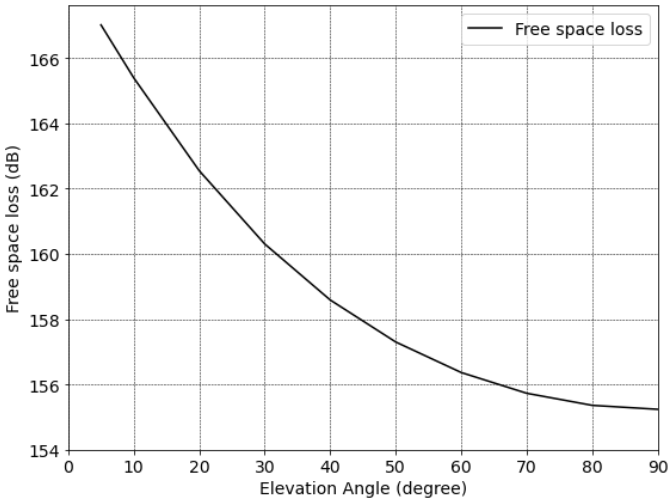

Fig.4. Free space loss depending on elevation angle.

The results for different data rates of 200 *kbit/s*, 500 *kbit/s*, and 1.5 *Mbit/s* are shown in Figure 5. The E_b/N_o level for the 1.5 *Mbit/s* bit rate exceeds 20 *dB* at the nadir position and decreases to 5 *dB* at the 10-degree elevation angle. The required E_b/N_0 level for 8PSK2/3 MODCOD should exceed 3.65 *dB* for reliable radio communication according to the DVB-S2 standard. Consequently, the transmission rate of 1.5 *Mbit/s* based on the 8PSK2/3 signal configuration can be maintained practically from the moment the satellite appears on the horizon. The E_b/N_o ratio for 200 *kbps* is 13 *dB* at a 10-degree elevation angle and grows to 30 *dB* at the nadir position, considerably exceeding the threshold for QPSK modulation. Consequently, low-

speed data transmission of telemetry data can be performed using either simple QPSK modulation or according to the broadcasting standard.

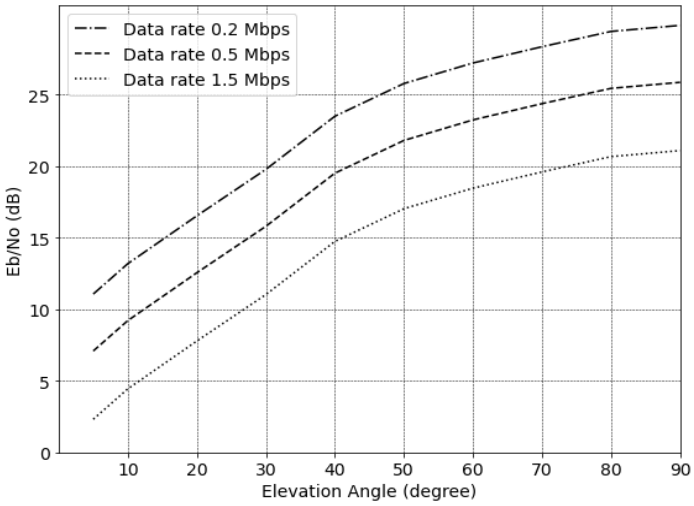

Fig.5. Calculated E_b/N_o for different data rates for downlink.

The radio link budget is estimated for the uplink based on the following parameters: the EIRP of the ground station is 44.5 *dB*, the operating frequency is 2.1 *GHz*, the orbit altitude is 600 km. The same patch antenna used for the downlink is also used as the receiving satellite antenna. The calculated G/T of the receiving antenna is demonstrated in Figure 6. The signal attenuation due to free-space propagation is close to the values obtained for the downlink due to the close operating frequencies.

The calculated E_b/N_o which is required for different bit rates of 50 *kbit/s*, 100 *kbit/s* and 200 *kbit/s* are shown in Figure 7. As it can be observed, under these communication conditions, obtained level of Eb/No is close to 15 *dB* at elevation angle of 5 degrees for a bit rate of 200 *kbit/s*. Transmission of telecommands is carried out on CPFSK modulation, for which the required level of E_b/N_o is 13.6 *dB* at BER = 10^{-6}. Consequently, the data rate of 200 *kbit/s* can be supported practically at any elevation angle from the horizon. However, the rate of 200 *kbit/s* is much higher than the typical telecommand rates in the range of 20-60 *kbps*. Thus, we can conclude that the considered communication channel has a significant power margin.

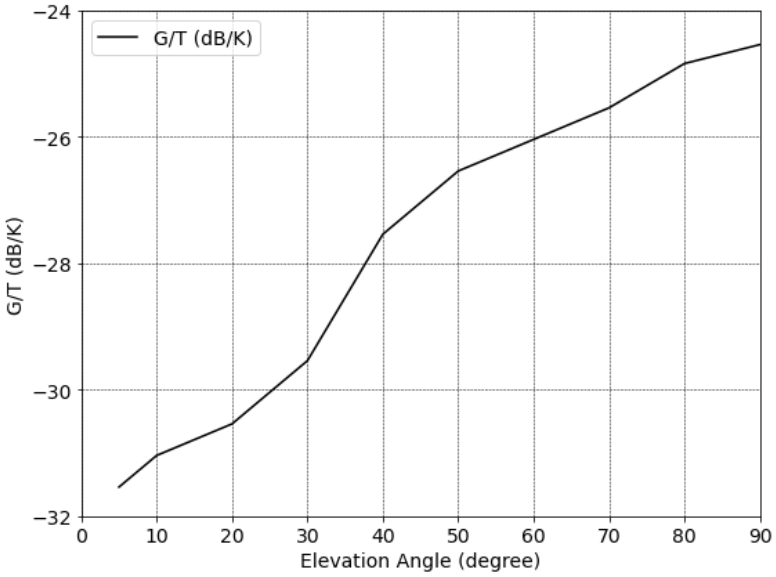

Fig.6. Calculated G/T of receiving satellite antenna depending on elevation angle.

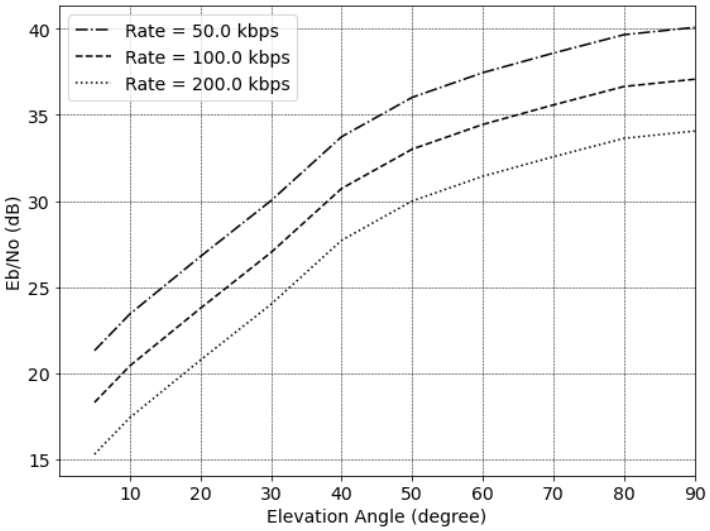

Fig.7. Calculated E_b/N_o for different data rates for uplink.

4. Conclusions

It is shown that the developed SDR transceiver using FPGA provides greater flexibility and allows it to be used in multiple frequency bands, filtering, adaptive modulation and encoding schemes without significant changes in hardware.

Advanced coding and modulation schemes are implemented in the DVB-S2 standard to reduce the required E_b/N_o level and achieve higher data rates without increasing signal power.

The E_b/N_o values were calculated for a ground station depending on the elevation angle at different transmission rates, taking into account atmospheric losses and power reserves, which make it possible to determine the ratio of the transmitter output power level and the antenna gain depending on the data transmission rate requirement.

The calculated data and S-band transceiver described in this article will be used for a ground station that provides services for a constellation of nanosatellites for Earth remote sensing, communications or IoT.

Conflict of interest statement

The authors declare that they have no conflict of interest in relation to this research, whether financial, personal, authorship or otherwise, that could affect the research and its results presented in this paper.

CRediT author statement

Baktybekov K.S.: Conceptualization, Supervision - Original Draft; **Bochkova E.N.:** Writing - Review & Editing; **Korol V.V**.: Data Curation – Writing; **Murushkin M.S.:** Data Curation, Writing; **Zhumazhanov B.R.:** Writing - Review.
The final manuscript was read and approved by all authors.

Acknowledgments

This research has been/was/is funded by the Aerospace Committee of the Ministry of Digital Development, Innovations and Aerospace Industry of the Republic of Kazakhstan (BR 21982462)

References

1 Liashkevich S.V., Saetchnikov V.A. (2021) SDR Based X-Band University Ground Station as Remote Sensing Technologies Learning Environment. *Proceeding of the 8th International Workshop on Metrology for AeroSpace*, IEEE Xplore, 127 – 131. DOI: 10.1109/MetroAeroSpace51421.2021.9511743.

2 Reinhart R., Lux J.P. (2014) Space-based reconfigurable software defined radio test bed aboard international space station. *Proceeding of the "SpaceOps" conference*, AIAA 2014-1612. DOI: 10.2514/6.2014-1612.

3 Ferreira P.V.R., Paffenroth R., Wyglinski A.M., Hackett T.M.; Sven G. Bilen S.G., Reinhart R.C. (2019) Reinforcement learning for satellite communications: From LEO to deep space operations. *IEEE Communications Magazine*, 57, 5, 70 – 75. DOI: 10.9/MCOM.2019.1800796.

4 Kozłowski S. (2018) A carrier synchronization algorithm for SDR-based communication with LEO satellite. *Radioengineering*, 27, 1, 299 – 306. DOI: 10.13164/re.2018.0299.

5 Ilco V., Levineț N., Gîrșcan., A. Margarint, A., Secrieru N. (2015) *Satellite telemetry data reception and processing via software defined radio.* Available at: http://repository.utm.md/handle/5014/2351.

6 Grayver E., Chin A., Hsu J., Stanev S., Kun D., Parower A. (2015) Software defined radio for small satellites. *Proceeding of the IEEE Aerospace Conference*, 1 – 9. DOI: 10.1109/AERO.2015.7118901.

7 Ceylan O., Caglar A., Tugrel H.B., Cakar O., Kislal A.O., Kula K., Yagci H. B. (2016) Satellites. *IEEE icrowave magazine,* 17, 3, 26 – 33. DOI: 10.1109/MMM.2015.2505700.

8 Guerra A.G.C., Ferreira A.S., Costa M., Nodar-Lopez D., Agelet F.A. (2018) Integrating ´ small satellite communication in an autonomous vehicle network: A case on oceanography. *Acta Astronautica,* 145, 229 – 237. DOI:10.1016/j.actaastro.2018.01.022.

9 Maheshwarappa M.R. (2016) *Software defined radio (SDR) architecture for concurrent multisatellite communications.* PhD dissertation. University of Surrey. Available at: https://openresearch.surrey.ac.uk/esploro/outputs/doctoral/Software-defined-radio-SDR-architecture-for/99511622502346.

10 Juang J.C., Tsai C.T., Miau J.J. (2008) A software-defined radio approach for the implementation of ground station receivers. In book: *Small Satellites for Earth Observation,* 293–298. DOI: 10.1007/978-1-4020-6943-7.

11 Quintana-Dıaz G., Birkeland R. (2018) Software-Defined Radios in Satellite Communications. *Proceeding of the conference ESA 4S Symposium*, Sorrento, Italy. Available at: https://www.researchgate.net/publication/330398017.

12 Ajith Kumar Joel, Pavan Kalyan Redd, Charan Yadav, Chandan M., Devanathan M. (2020) SDR Based Ground Station for Image Reception from Weather Satellites. *International Journal of Advance Science and Technology*, 29, No. 10S, 7694 – 7705. Available at: https://sersc.org/journals/index.php/IJAST/article/view/24092.

13 Velasco C., Tipantuña C. (2017) Meteorological picture reception system using software defined radio (SDR). *Proceeding of the IEEE 2nd Ecuador Technical Chapters Meeting*, 1-6. DOI: 10.1109/ETCM.2017.8247551.

14 Georgescu I., Angelescu N., Puchianu D.C., Predusca G., Circiumarescu L-D. (2021) Software defined radio applications-receiving and decoding images transmitted by weather satellites. *Proceeding of the 13th Intern. Conf. on Electronics, Computers and Artificial Intelligence*, 1 – 4. DOI: 10.1109/ECAI52376.2021.9515169.

15 Thabit A.A. (2020) Design and software implementation of radio frequency satellite link based on SDR under noisy channels. *Telkomnika*, 8, 6, 2852 - 2860. DOI: 10.12928/telkomnika.v18i6.16130.

16 Halté S., Chambon C., Rawson S., Dasgupita A., Neveux G., Barataud D. (2019) X-band sampling technology demonstration. *Proceeding of the TTC 2019 - 8th ESA International Workshop on Tracking, Telemetry and Command Systems for Space Applications, IEEE Xplore.* DOI: 10.1109/TTC.2019.8895295.

17 Chen W., Khan A.Q., Abid M., Ding S. (2011) Integrated design of observer-based fault detection for a class of uncertain nonlinear systems. *International Journal of Applied Mathematics and Computer Science,* 21(3), 423 – 430. DOI:10.2478/v10006-011-0031-0.

18 Pratt T., Bostian C., Allnutt J. *Satellite Communications.* Wiley, 560. Available at: https://books.google.com/books/about/Satellite_Communications.h tml?id=IqFvngEACAAJ2002.

19 Larson W.J., Wertz A.V. (1992) *Space Mission Analysis and Design.* Springer, 976, 381 – 395. Available at: https://books.google.com/books/about/Space_Mission_Analysis_and_Design.html?id=QJanyiWfvXMC.

20 Benvenuto N., Cherubini G. (2002) *Algorithms for Communications Systems and Their Applications*. John Wiley & Sons. 508. Available at: https://lib.ysu.am/open_books/413038.pdf.

21 Joseph A. Shaw. (2013) Radiometry and the Friis transmission equation. *Am. J. Phys.*, 81, 33 – 37. DOI:10.1119/1.4755780.

AUTHORS' INFORMATION

Baktybekov, Kazbek S. – Doctor of Phys. & Math. Sciences, Professor, Department of Advanced and Research Projects, Leading Design Engineer, Ghalam LLP, Astana, Kazakhstan; Scopus Author ID: 8926833000, ORCID: 0000-0002-6401-8053; k.baktybekov@ghalam.kz

Bochkova, Elena Nikolaevna – PhD, Department of Ground Complex and Technical Support, Leading Design Engineer, Ghalam LLP, Astana, Kazakhstan; Scopus Author ID: 56820098200; ORCID: 0000-0003-4851-306X; e.bochkova@ghalam.kz

Korol, Vladimir Viktorovich – PhD, Department of Design and Technical Analysis, Leading Design Engineer, Ghalam LLP, Astana, Kazakhstan; ORCID: 0009-0000-4081-1316; v.korol@ghalam.kz

Murushkin, Mikhail Sergeevich – PhD, Special Design Bureau of Space Technology, Leading Design Engineer, Ghalam LLP, Astana, Kazakhstan; ORCID: 0009-0006-9917-3842; m.murushkin@ghalam.kz

Zhumazhanov Berik Rakhymbekuly - Head of the Office of Advanced and Research Projects, Ghalam LLP, Astana, Kazakhstan, Scopus Author ID: 57350754500; ORCID: 0000-0001-5926-9619; b.zhumazhanov@ghalam.kz